PHYSICAL REVIEW B **96**, 121202(R) (2017)

Photodynamics of quantum emitters in hexagonal boron nitride revealed by low-temperature spectroscopy

Bernd Sontheimer,[1,*] Merle Braun,[1] Niko Nikolay,[1] Nikola Sadzak,[1] Igor Aharonovich,[2] and Oliver Benson[1]

[1]*Institut für Physik, Humboldt-Universität zu Berlin, Newtonstrasse 15, D-12489 Berlin, Germany*

[2]*School of Mathematical and Physical Sciences, University of Technology Sydney, Ultimo, NSW 2007, Australia*

(Received 19 April 2017; published 18 September 2017)

Quantum emitters in hexagonal boron nitride (hBN) have recently emerged as promising bright single photon sources. In this Rapid Communication we investigate in detail their optical properties at cryogenic temperatures. In particular, we perform temperature-resolved photoluminescence studies and measure photon coherence times from the hBN emitters. The obtained value of 81(1) ps translates to a width of ∼6.5 GHz which is higher than the Fourier transform limited value of ∼32 MHz. To account for the photodynamics of the emitter, we perform ultrafast spectral diffusion measurements that partially account for the coherence times. Our results provide important insight into the relaxation processes in quantum emitters in hBN which is mandatory to evaluate their applicability for quantum information processing.

DOI: 10.1103/PhysRevB.96.121202

Single photon sources (SPSs) are prime candidates for myriad applications in integrated quantum photonics, quantum optics, and information processing [1–4]. Fluorescent atomic defects in solids (atomlike emitters) are particularly attractive in this regard as they offer exciting opportunities for scalable quantum networks. Several systems have been investigated in detail, including rare earth ions in solids [5,6], defects in silicon carbide (SiC) [7–9], defect centers in diamond such as the nitrogen vacancy (NV) [10,11], the silicon vacancy (SiV) [12–15], and more recently the germanium vacancy (GeV) [16–19]. Latterly, a new family of SPSs emerged in hexagonal boron nitride (hBN) [20–26]. hBN is a wide-band-gap material (ca. 6 eV) and can therefore host fluorescent defect centers that can be triggered at room temperature using a subband-gap excitation [27]. While the origin of the emitters is still under debate, it is tentatively associated with the antisite nitrogen vacancy (N_BV_N) [21]. At room temperature these emitters exhibit remarkable properties including high brightness, polarization, and short excited state lifetime, making them promising candidates for quantum technologies.

In this Rapid Communication we investigate in details the optical properties of single emitters in hBN at cryogenic temperatures to understand the electron phonon processes and the dephasing mechanisms. In particular, we present interferometric measurements of quantum emitters in two-dimensional materials. First, we cool down the selected emitter and observe the change in linewidth and central position. At 5 K we then perform lifetime and first-order coherence measurements to further quantify optical dephasing mechanisms. We further find the time scale of an apparent spectral diffusion process that causes the line to be spectrally much broader than the natural linewidth. These measurements are of a high importance for understanding of their photophysical, structural, and optical properties.

The experiments are conducted with a home-built confocal microscope, sketched in Fig. 1(a), to selectively excite defects in hBN flakes. The sample preparation was adapted from Ref. [21]. In the setup, collected photons are guided through a Michelson interferometer which allows for measurements of the photon coherence time τ_c as well as the spectral diffusion time τ_d. By blocking one of the interferometer arms, the detection path is effectively converted to a Hanbury Brown and Twiss configuration for standard second-order correlation measurements (correlation electronics: PicoHarp300, PicoQuant). By redirecting the detection path from one of the avalanche photodiodes (APDs, Count20, Laser Component) to a spectrometer (SP500i, Princeton Instruments), spectra can be measured while conveniently locking on the emitter intensity with the other APD. The emitters themselves, as well as the objective lens [numerical aperture (NA) 0.9, Mitutoyo], are placed inside a liquid helium flow cryostat (CryoVac). This enables for highly efficient photon collection during the sample cooldown from 300 to 5 K. At cryogenic temperatures a pair of widely tunable long and short pass filters (704 nm VersaChrome Edge, Semrock) acts as a ∼5 nm bandpass centered at the zero phonon line (ZPL) of the selected single emitter, to maximize the signal-to-background ratio. An additional 620-nm long pass filter and the dichroic mirror further suppress the 532-nm excitation diode laser. Lifetime measurements were performed using a picosecond pulsed 532-nm laser (LDH-P-FA-530, PicoQuant). In accord with recent research [21–24] we find a broad variation of the optical properties of hBN emitters. For the following experiments we selected an emitter that showed a stable ZPL at room temperature [Fig. 1(b)] and a clear antibunching dip [Fig 1(c)]. In total, all measurements were performed on the same defect over the course of 2 days, during which it was constantly tracked and proved to be stable.

Figure 2(a) shows a heat map of the spectra recorded during the cooling process. Each individual spectrum was integrated for 500 ms. The temperature resolution was limited to 0.1 K and spectra within each temperature step were averaged, in order to obtain an optimal signal-to-noise ratio. Cooling from room temperature to 5 K took about 1 h and the cooling rate was kept constant. Down to a temperature of 20 K the line shape and position of the ZPL significantly change. To further investigate on those changes we follow the approach given in Ref. [28]: In general, the ZPL shape is governed by

*bernd.sontheimer@physik.hu-berlin.de; www.physik.hu-berlin.de/nano

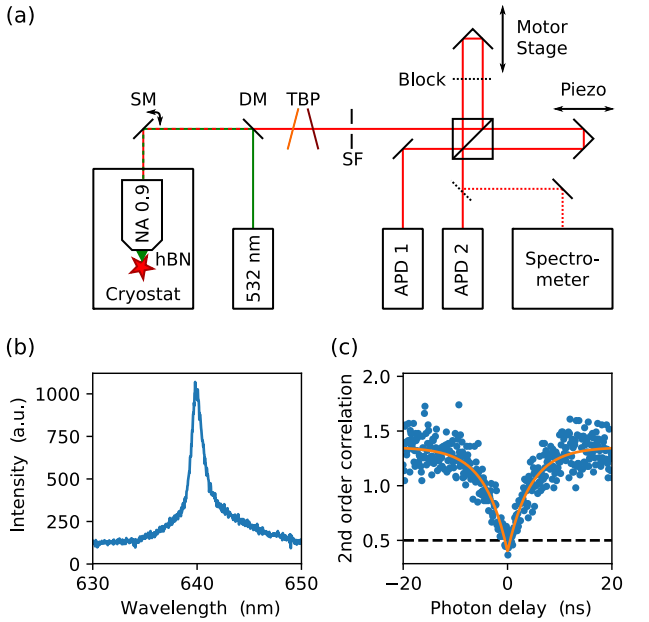

FIG. 1. Setups and basic characterization. (a) Schematic of the experimental setup. SM: x/y-scanning mirrors; DM: dichroic mirror; TBP: tunable bandpass consisting of a long and a short pass filter; SF: spatial, confocal filtering system. By blocking one interferometer arm the detection path effectively becomes a typical Hanbury Brown and Twiss configuration for second-order correlation measurements. One output of the beam splitter can be directed to the spectrometer, allowing for convenient emitter tracking during spectral measurements. (b) Room-temperature spectrum of a single photon emitter in hBN. (c) Closeup of the $g^{(2)}$ function around $\tau = 0$ shows typical single photon antibunching behavior with $g^{(2)}(0) < 0.5$. [Blue: data; orange: fit; black dashed: $g^{(2)}(\tau) = 0.5$.]

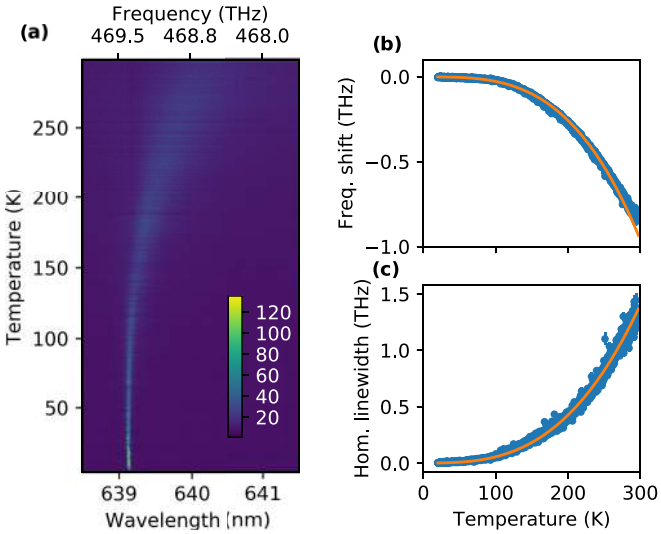

FIG. 2. Temperature-dependent measurements: (a) Spectra, (b) frequency shift, and (c) homogeneous linewidth of the ZPL. The values in (b) and (c) are extracted from fits to a Lorentzian model following the approach from Ref. [28]. The solid lines in (b) and (c) are fits to a power law, resulting in a $T^{3.39(1)}$ and $T^{2.94(1)}$ dependency, respectively.

homogeneous and inhomogeneous broadening mechanisms, which lead to a Lorentzian and Gaussian shape, respectively. For defect centers in solid states the predominant mechanisms are spectral diffusion (inhomogeneous) and phonon broadening (homogeneous) [28–31]. If both occur, the resulting line shape is given by the convolution of both—a Voigt profile,

$$I_V(\nu) = \frac{A\,\mathrm{Re}[w(z)]}{\sigma\sqrt{2\pi}}, \tag{1}$$

with

$$w(z) = e^{-z^2}\,\mathrm{erfc}(-iz) \quad \text{and} \quad z = \frac{\nu - \mu + i\gamma}{\sigma\sqrt{2}}, \tag{2}$$

where A is the peak amplitude, μ is the center, $f_G = 2\sigma\sqrt{2\ln 2}$ is the full width at half maximum of the Gaussian contribution, and $f_L = 2\gamma$ is the full width at half maximum of the Lorentzian contribution. In the following discussion, the obtained linewidths were corrected for the spectrometer response function, which also follows a Voigt profile (see Supplemental Material [32]). In agreement with other defect centers in broad band-gap semiconductors [28,30], we see a transition from a predominantly Gaussian line shape to a Lorentzian-like spectrum for increasing temperatures. In analogy to defects in nanodiamond [28,29], this indicates that the phonon broadening increases with temperature while the spectral diffusion stays mostly temperature independent. In order to fit the measured spectra to theoretical Voigt profiles we adapt the procedure established for silicon vacancy centers in diamond described in Ref. [28]: At low temperatures the Lorentzian width of the measured Voigt profiles is assumed to be far below the spectrometer resolution and therefore is fixed to the value obtained from the spectrometer response function $f_{L,\mathrm{spec}} = 3.7$ GHz. For up to 20 K fits to the measured profiles yield a constant value of $f_G = 21.3$ GHz. This is the temperature-independent spectral diffusion linewidth. For higher temperatures the Gaussian width is fixed to this value and f_L is left as an unrestrained fit parameter. The graphs in Figs. 2(b) and 2(c) show a shift of the central frequency and a broadening of the homogeneous linewidth extracted from the resulting fits for all temperatures. The frequency redshift follows a power law proportional to $T^{3.39(1)}$. This compares well with measurements on SiV and chromium defect centers in diamond, where a T^3-dependent shift is commonly attributed to fluctuating fields which are created as a phonon modulates the distance between the color center and other impurities in the crystal [28,30]. For the linewidth we observe a broadening with a $T^{2.94(1)}$ power law for increasing temperatures. Again, this is similar to the behavior found in the diamond defects mentioned above. Moreover, a power law close to T^3 for the linewidth was observed in solid state systems exhibiting significant inhomogeneous ZPL broadening [33,34], where it was also linked to the influence of impurities in the host material [35]. This corresponds well with our results, since the two-dimensional nature of hBN implies a rather unprotected environment for the embedded defect center.

Next, we explore the actual limit of the single hBN defect at low temperature. A measurement of the excited state lifetime τ [Fig. 3(a)] reveals a natural linewidth $f_n = (2\pi\tau)^{-1} \approx 32$ MHz. This ultimate limit is far below the

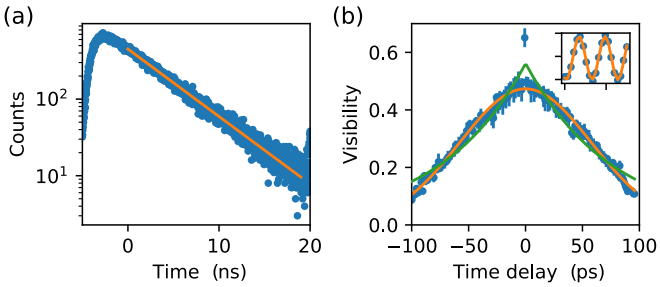

FIG. 3. Lifetime and coherence measurements of a single defect in hBN. (a) Lifetime measurement [blue: data; orange: exponential fit with $\tau = 4.93(2)$ ns]. (b) Measured first-order coherence measurement [blue: data; green: exponential fit with $\tau_{c,e} = 76(2)$ ps; orange: Gaussian fit with $\tau_{c,G} = 81(1)$ ps]. Each visibility data point is the result of a fit to a piezoscan of about two fringes during 250 ms at a fixed stage position (inset).

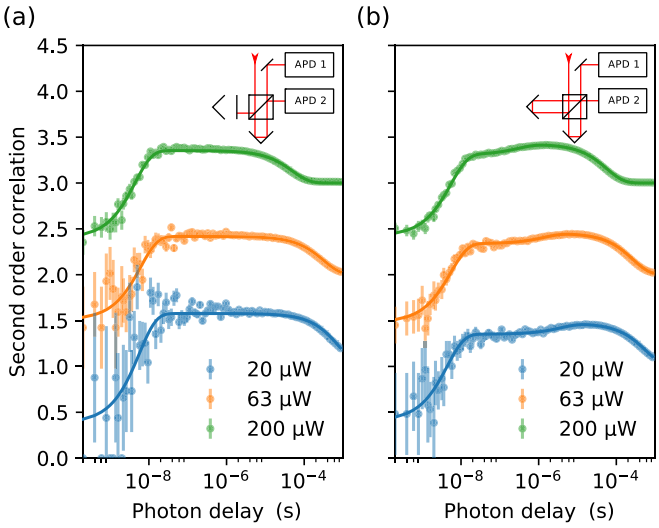

FIG. 4. Second-order correlations of the emitter signal for different excitation laser powers with (a) detection in a typical Hanbury Brown and Twiss configuration and (b) detection at the output ports of a Michelson interferometer. While (a) follows the $g^{(2)}$ function of a three-level system, (b) additionally shows the effect of spectral diffusion. For each measurement data were collected for 10 min. The error bars correspond to the square root of the coincidence events within each time bin. (Points with error bars: correlated data; solid lines: fits; the orange and green curves have an offset of +1 and +2, respectively.)

spectrometer resolution. However, interferometric measurements can resolve much narrower lines. We therefore perform first-order coherence measurements on the ZPL at 5 K with the Michelson interferometer illustrated in Fig. 1(a). Figure 3(b) shows the obtained interference visibility as a function of the relative time delay due to the interferometer path length difference. For each data point the motor stage was moved to a specific delay position and the interferogram was measured locally by scanning the piezo over roughly two interference fringes [Fig. 3(b) inset]. The visibility was then extracted by fitting a sine function with an offset to the interferogram and calculating the absolute value of the quotient of the resulting oscillation amplitude and the offset. From Fig. 3(b) we identify a Gaussian-like visibility profile centered at the position of equal interferometer arm lengths. This is in very good agreement with the predominantly Gaussian emitter line shape at cryogenic temperatures already seen in the photoluminescence spectrum [36]. In contrast, homogeneous broadening mechanisms such as phonon coupling would result in a Lorentzian-like spectral line and an exponentially decaying visibility profile [36].

The coherence time of 81(1) ps corresponds to a spectral width of $f_c = 2\sqrt{\ln(2)}/(\pi\tau_c) \approx 6.5$ GHz [36], roughly 200 times wider than the Fourier limited linewidth. This measurement represents a linewidth measurement from a single emitter in a two-dimensional material and especially hBN. Although this is still far from the Fourier limit, we would like to point out that the value is comparable to or even better than the ones obtained from measurements on chromium or NV centers in diamond [30,37].

As seen above, the main reason for the large difference between the lifetime limited width and the one obtained with the spectrometer and interferometer is inhomogeneous broadening. In the following we investigate further on the underlying mechanism: We propose spectral jumps. If many of those jumps occur during the data acquisition (typically 250 ms for both measurement types), they are effectively averaged and result in a broadened linewidth. We can confirm the presence and determine the time scale of spectral jumps with second-order correlation measurements following the approach demonstrated in Ref. [29]. Photons emitted from the hBN defect follow the $g^{(2)}$ function of a three-level system

$$g^{(2)}(\tau) = 1 - (1 + A)e^{-\frac{\tau}{t_1}} + A\,e^{-\frac{\tau}{t_2}}, \tag{3}$$

with the bunching amplitude A, the antibunching time t_1, and the bunching time t_2. In the experiment we measure the $g^{(2)}$ function by blocking one arm of the Michelson interferometer [see Fig. 4(a) inset] and correlating the APD signal. This resembles a typical Hanbury Brown and Twiss configuration. The treatment of additional background with a Poissonian photon statistic is described in the Supplemental Material [32]. With the interferometer arm unblocked, the measurement is additionally modified by the presence of the interferometer, which transforms frequency modulations, such as spectral diffusion, into intensity changes on the APDs. In this way even very fast spectral jumps can be resolved [29]. If the path length difference between the two arms of the interferometer and therefore the fringe width is smaller than the spectral diffusion width, the resulting $g^{(2)}_{LR}$ function reads as

$$g^{(2)}_{LR}(\tau) = \left(1 - \frac{c^2}{2}e^{\frac{\tau}{t_d}}\right)g^{(2)}(\tau), \tag{4}$$

where c is the interferometric contrast and t_d the spectral diffusion time [29]. Figure 4 shows the resulting second-order correlations for three different laser powers. Table I summarizes the relevant time parameters of the fits. For increasing powers, the antibunching time t_1 remains nearly unchanged at about 5 ns while the bunching time t_2 significantly reduces from 814(3) to 49.73(7) μs and respectively 575(1) to 56.59(3) μs for the different configurations. This behavior is typical for three-level systems [38,39]. The spectral diffusion

TABLE I. Selected fit parameters for fits in Fig. 4.

	Power (μW)	t_1 (ns)	t_2 (μs)	t_d (μs)
$g^{(2)}$	20	5 ± 1	814 ± 3	
	63	6.2±0.8	321.3±0.6	
	200	4.4±0.2	49.73±0.07	
$g^{(2)}_{LR}$	20	4.4±0.7	575.0±1.0	3.9±0.2
	63	5.5±0.3	268.4±0.2	1.4±0.5
	200	5.4±0.1	56.59±0.03	0.320±0.008

measurements show that t_d also decreases for increasing power from 3.9(2) to 0.320(8) μs, a trend that is also found for NV centers in nanodiamond [29]. However, this is still at least two orders of magnitude slower than the lifetime of the emitter, which means the defect emits multiple consecutive photons before it spectrally jumps.

The presence of the spectral diffusion is in accord with the potential defect structure of the nitrogen antisite that has a permanent dipole moment [21]. The rather fast values may suggest charging and discharging of the defect or charge traps in the emitter environment that will cause a small wavelength shift due to the dc Stark effect. The extra charge may originate from the rich nitrogen environment within the hBN lattice or, similar to NV centers in diamond [29], photoionized nearby impurities. The observed decreasing spectral diffusion time with increasing laser power further supports the latter assumption. Moreover, the presence of ultrafast spectral diffusion verifies again that the phonon coupling is not the dominant process causing the low coherence times. We also note that the recent development of engineering the hBN single emitters in large exfoliated materials can yield a more robust and clean environment that potentially reduces the spectral diffusion [23,25,40]. This is an analog to comparing emitters in nanodiamonds versus emitters in a bulk, that often exhibit many stable and superior photophysical properties. On the other hand, due to the two-dimensional nature of the host material, the defect is highly exposed to its surroundings. We therefore suspect the spectral diffusion to be strongly dependent on its close environment and therefore potentially applicable to very localized sensing applications.

To summarize, we presented a detailed characterization of an optically active point defect in hBN. We performed temperature-dependent photoluminescence experiments and measured the photon coherence time of the single photon emitter. The obtained photon coherence time 81(1) ps is still less than the lifetime limited value. This can be explained by the ultrafast spectral diffusion present in these emitters which causes an inhomogeneous broadening of the line. The presented results are important for further understanding of the hBN defect centers and lead to different ideas for quantum information and sensing applications based on two-dimensional wide-band-gap host materials.

We gratefully acknowledge funding from the DFG (Sfb 951) the Einstein Foundation Berlin (ActiPlAnt), and CNPq Brasil (science without borders program). We are also thankful for the financial support from the Australian Research Council (DE130100592) and the Asian Office of Aerospace Research and Development Grant No. FA2386-15-1-4044. Moreover, I.A. acknowledges support through a generous sponsorship provided by the Alexander von Humboldt Foundation.

[1] H. J. Kimble, Nature (London) **453**, 1023 (2008).
[2] P. Lodahl, S. Mahmoodian, and S. Stobbe, Rev. Mod. Phys. **87**, 347 (2015).
[3] T. D. Ladd, F. Jelezko, R. Laflamme, Y. Nakamura, C. Monroe, and J. L. O'Brien, Nature (London) **464**, 45 (2010).
[4] I. Aharonovich, D. Englund, and M. Toth, Nat. Photonics **10**, 631 (2016).
[5] T. Zhong, J. M. Kindem, E. Miyazono, and A. Faraon, Nat. Commun. **6**, 8206 (2015).
[6] R. Kolesov, K. Xia, R. Reuter, R. Stöhr, A. Zappe, J. Meijer, P. R. Hemmer, and J. Wrachtrup, Nat. Commun. **3**, 1029 (2012).
[7] S. Castelletto, B. C. Johnson, V. Ivády, N. Stavrias, T. Umeda, A. Gali, and T. Ohshima, Nat. Mater. **13**, 151 (2014).
[8] H. Kraus, V. A. Soltamov, D. Riedel, S. Väth, F. Fuchs, A. Sperlich, P. G. Baranov, V. Dyakonov, and G. V. Astakhov, Nat. Phys. **10**, 157 (2014).
[9] W. F. Koehl, B. B. Buckley, F. J. Heremans, G. Calusine, and D. D. Awschalom, Nature (London) **479**, 84 (2011).
[10] H. Bernien, B. Hensen, W. Pfaff, G. Koolstra, M. S. Blok, L. Robledo, T. H. Taminiau, M. Markham, D. J. Twitchen, L. Childress, and R. Hanson, Nature (London) **497**, 86 (2013).
[11] L. Childress and R. Hanson, MRS Bull. **38**, 134 (2013).
[12] A. Sipahigil, R. E. Evans, D. D. Sukachev, M. J. Burek, J. Borregaard, M. K. Bhaskar, C. T. Nguyen, J. L. Pacheco, H. A. Atikian, C. Meuwly, R. M. Camacho, F. Jelezko, E. Bielejec, H. Park, M. Lončar, and M. D. Lukin, Science **354**, 847 (2016).
[13] J. N. Becker, J. Görlitz, C. Arend, M. Markham, and C. Becher, Nat. Commun. **7**, 13512 (2016).
[14] T. Müller, C. Hepp, B. Pingault, E. Neu, S. Gsell, M. Schreck, H. Sternschulte, D. Steinmüller-Nethl, C. Becher, and M. Atatüre, Nat. Commun. **5**, 3328 (2014).
[15] Y. Zhou, A. Rasmita, K. Li, Q. Xiong, I. Aharonovich, and W.-b. Gao, Nat. Commun. **8**, 14451 (2017).
[16] T. Iwasaki, F. Ishibashi, Y. Miyamoto, Y. Doi, S. Kobayashi, T. Miyazaki, K. Tahara, K. D. Jahnke, L. J. Rogers, B. Naydenov, F. Jelezko, S. Yamasaki, S. Nagamachi, T. Inubushi, N. Mizuochi, and M. Hatano, Sci. Rep. **5**, 12882 (2015).
[17] E. A. Ekimov, S. G. Lyapin, K. N. Boldyrev, M. V. Kondrin, R. Khmelnitskiy, V. A. Gavva, T. V. Kotereva, and M. N. Popova, JETP Lett. **102**, 701 (2015).
[18] P. Siyushev, M. H. Metsch, A. Ijaz, J. M. Binder, M. K. Bhaskar, D. D. Sukachev, A. Sipahigil, R. E. Evans, C. T. Nguyen, M. D. Lukin, P. R. Hemmer, Y. N. Palyanov, I. N. Kupriyanov, Y. M. Borzdov, L. J. Rogers, and F. Jelezko, Phys. Rev. B **96**, 081201(R) (2017).
[19] M. K. Bhaskar, D. D. Sukachev, A. Sipahigil, R. E. Evans, M. J. Burek, C. T. Nguyen, L. J. Rogers, P. Siyushev, M. H. Metsch, H. Park, F. Jelezko, M. Lončar, and M. D. Lukin, Phys. Rev. Lett. **118**, 223603 (2017).
[20] T. T. Tran, K. Bray, M. J. Ford, M. Toth, and I. Aharonovich, Nat. Nanotechnol. **11**, 37 (2016).

[21] T. T. Tran, C. Elbadawi, D. Totonjian, C. J. Lobo, G. Grosso, H. Moon, D. R. Englund, M. J. Ford, I. Aharonovich, and M. Toth, ACS Nano **10**, 7331 (2016).

[22] N. R. Jungwirth, B. Calderon, Y. Ji, M. G. Spencer, M. E. Flatté, and G. D. Fuchs, Nano Lett. **16**, 6052 (2016).

[23] N. Chejanovsky, M. Rezai, F. Paolucci, Y. Kim, T. Rendler, W. Rouabeh, F. Fávaro de Oliveira, P. Herlinger, A. Denisenko, S. Yang, I. Gerhardt, A. Finkler, J. H. Smet, and J. Wrachtrup, Nano Lett. **16**, 7037 (2016).

[24] R. Bourrellier, S. Meuret, A. Tararan, O. Stéphan, M. Kociak, L. H. G. Tizei, and A. Zobelli, Nano Lett. **16**, 4317 (2016).

[25] A. L. Exarhos, D. A. Hopper, R. R. Grote, A. Alkauskas, and L. C. Bassett, ACS Nano **11**, 3328 (2017).

[26] A. W. Schell, H. Takashima, T. T. Tran, I. Aharonovich, and S. Takeuchi, ACS Photonics **4**, 761 (2017).

[27] L. H. Li and Y. Chen, Adv. Funct. Mater. **26**, 2594 (2016).

[28] E. Neu, C. Hepp, M. Hauschild, S. Gsell, M. Fischer, H. Sternschulte, D. Steinmüller-Nethl, M. Schreck, and C. Becher, New J. Phys. **15**, 043005 (2013).

[29] J. Wolters, N. Sadzak, A. W. Schell, T. Schröder, and O. Benson, Phys. Rev. Lett. **110**, 027401 (2013).

[30] T. Müller, I. Aharonovich, Z. Wang, X. Yuan, S. Castelletto, S. Prawer, and M. Atatüre, Phys. Rev. B **86**, 195210 (2012).

[31] K.-M. C. Fu, C. Santori, P. E. Barclay, L. J. Rogers, N. B. Manson, and R. G. Beausoleil, Phys. Rev. Lett. **103**, 256404 (2009).

[32] See Supplemental Material at http://link.aps.org/supplemental/10.1103/PhysRevB.96.121202 for the spectrometer response function and $g^{(2)}$-function background treatment.

[33] C. Wei, K. Holliday, A. J. Meixner, M. Croci, and U. P. Wild, J. Lumin. **50**, 89 (1991).

[34] J. Krustok, J. Raudoja, and R. Jaaniso, Appl. Phys. Lett. **89**, 051905 (2006).

[35] V. Hizhnyakov, H. Kaasik, and I. Sildos, Phys. Status Solidi B **234**, 644 (2002).

[36] T. Salamon, Acta Phys. Acad. Sci. Hung. **36**, 269 (1974).

[37] F. Jelezko, A. Volkmer, I. Popa, K. K. Rebane, and J. Wrachtrup, Phys. Rev. A **67**, 041802 (2003).

[38] E. Neu, M. Agio, and C. Becher, Opt. Express **20**, 19956 (2012).

[39] M. W. Doherty, N. B. Manson, P. Delaney, F. Jelezko, J. Wrachtrup, and L. C. L. Hollenberg, Phys. Rep. **528**, 1 (2013).

[40] S. Choi, T. T. Tran, C. Elbadawi, C. Lobo, X. Wang, S. Juodkazis, G. Seniutinas, M. Toth, and I. Aharonovich, ACS Appl. Mater. Interfaces **8**, 29642 (2016).